Journal of Alloys and Compounds 666 (2016) 243–247

Contents lists available at ScienceDirect

Journal of Alloys and Compounds

journal homepage: http://www.elsevier.com/locate/jalcom

$Fe_{83}P_{15}Cu_1Al_1$ partial nanocrystalline alloy obtained by one-step melt spinning method

J.S. Zhu, Y.G. Wang*, G.T. Xia, J. Dai, J.K. Chen

College of Materials Science and Technology, Nanjing University of Aeronautics and Astronautics, Nanjing, 210016, People's Republic of China

ARTICLE INFO

Article history:
Received 17 November 2015
Received in revised form
7 January 2016
Accepted 8 January 2016
Available online 13 January 2016

Keywords:
Crystallization
Nanocrystalline alloys
Amorphous alloys
Soft magnetic properties

ABSTRACT

Soft magnetic alloy $Fe_{83}P_{16-x}Cu_1Al_x$ ($x = 0$–1.5) ribbons were produced by the single roller melt spinning method. The effect of Al content on the glass forming ability, thermal stability, mechanical properties and soft magnetic properties was investigated. Melt-spun $Fe_{83}P_{15}Cu_1Al_1$ nanocrystalline alloy exhibits good soft magnetic properties, such as high saturation magnetic flux density (1.62 T) and low coercivity (12.9 A/m) and good mechanical properties, such as the hardness (11.9 GPa) and the Young's modulus (248.2 GPa). The special mechanism for obtaining this partial nanocrystalline alloy without annealing is discussed based on the crystallization activation energy.

© 2016 Elsevier B.V. All rights reserved.

1. Introduction

Fe-based nanocrystalline soft magnetic materials play an important role in magnetic devices such as transformers and inductors [1–3]. They are usually produced by crystallization of rapidly quenched amorphous ribbons and have, meanwhile, become an established industrial product [4]. To increase the saturation magnetization toward the value of that of FeSi steel is becoming a major driving force in search for competitive alloy compositions. However, with the increase of iron content the glass forming ability (GFA) decreases sharply becoming the major hindrance towards the development of amorphous precursors. For the traditional FINEMET alloys in order to obtain amorphous precursors with excellent GFA certain amount of B addition is necessary [5–7]. Refractory metals with large atomic radius such as Nb [8], Mo [9] and Zr [7,10] are also indispensible. However, these elements are all expensive and, as a result, the addition of one or more of them will increase the production cost which limits the mass application of these alloys. We have successfully fabricated a new kind of nanocrystalline soft magnetic alloy $Fe_{83}P_{16}Cu_1$ with a simple and cheap alloy composition [11]. In this study, P was partly substituted by Al in the $Fe_{83}P_{16}Cu_1$, and soft magnetic alloys with partial nanocrystalline can be obtained directly by melt spinning without the following annealing. The nanocrystalline grains disperse inhomogeneously in the amorphous substrate. The melt-spun ribbons still possess good mechanical property similar to amorphous ones and show good soft magnetic properties. Dependences of the GFA, the thermal stability, the crystallization process, mechanical property and soft magnetic properties on Al content in $Fe_{83}P_{16-x}Cu_1Al_x$ alloy ribbons were investigated.

2. Experimental details

Fe-based alloy ingots with the nominal composition of $Fe_{83}P_{16-x}Cu_1Al_x$ ($x = 0$, 0.5, 1, 1.5) were prepared by arc-melting a mixture of industry raw materials: Fe (99.9%), P–Fe (P: 26.11%, Fe: 71.85%), Cu (99.99%), and Al (99.6%) under argon atmosphere. All the ingots were remelted four times and stirred by magnetic beater to ensure homogeneity in a Ti-gettered argon atmosphere. Ribbons with a width of about 1.5 mm and thickness of about 25 μm were produced by single-roller melt spinning method at an argon atmosphere onto a copper wheel with circumferential speed of 40 m/s. Thermal properties of melt-spun ribbons were evaluated with a differential scanning calorimeter (DSC) under argon flow. The microstructure of melt-spun and annealed ribbons was examined by x-ray diffraction (XRD) with Cu-Kα radiation ($\lambda = 1.54056$ Å) and by transmission electron microscopy (TEM). The composition of the samples was analyzed with Energy Dispersive Spectrometer (EDX). The hardness and Young's modulus were obtained from nano-indentation. The coercivity H_C and magnetic flux density of the

* Corresponding author.
E-mail address: yingang.wang@nuaa.edu.cn (Y.G. Wang).

http://dx.doi.org/10.1016/j.jallcom.2016.01.055
0925-8388/© 2016 Elsevier B.V. All rights reserved.

samples were determined from analysis of B–H loop tracer with the maximum magnetizing field of 8000 A/m.

3. Results and discussion

Fig. 1(a) and (b) show the XRD patterns taken from the free side and the wheel side of the as-quenched ribbons for $Fe_{83}P_{16-x}Cu_1Al_x$ ($x = 0, 0.5, 1, 1.5$) alloys denoted as S1, S2, S3 and S4, respectively. Broad peaks at about $2\theta = 45^\circ$ can be seen from XRD patterns in Fig. 1(a), which indicates that S1 is amorphous structure. However, with the addition of 0.5 at. % Al, the diffraction pattern shows two reflection peaks: the first, broad peak, is caused by the amorphous phase and the second, sharp peak at $2\theta \approx 66^\circ$, is related to the (200)-reflection of a crystalline α-Fe phase [12,13]. As the Al content increases to 1 at. %, the second peak disappears and the peak at about $2\theta = 45^\circ$ corresponding to (110) of α-Fe phase turns to be clear. For S4 two clear peaks corresponding to α-Fe phase [14] appear which indicates that crystallization phases appear intensively with further addition of Al. From Fig. 1(b), one can find that the wheel side of S1, S2 and S3 are with amorphous structure and S4 becomes partially crystallized. Therefore, one can infer that GFA deteriorates with the addition of Al. We also demonstrated that the substitution of 2 at. % Al for P would embrittle the alloy ribbon. Therefore we only investigate alloys with Al below 1.5 at. %. EDX spectra from both sides of the ribbons (not shown here) indicate that the composition appears no clear difference. The difference of structures between the two sides results from the differences of the cooling rate. The alloy composition in this work is on the Fe-rich side of the eutectic reaction based on the Fe–P binary phase diagram [15]. According to the phase selection principle [16,17], only α-Fe phase appears on the amorphous matrix.

Thermal stability of the samples was investigated by analyzing the DSC curves. Fig. 2(a) shows DSC curves of $Fe_{83}P_{16-x}Cu_1Al_x$ ($x = 0$–1.5) alloy ribbons with a heating rate of 10 K/min in an Ar flow. Two obvious exothermic peaks corresponding to two different crystallization phases are detected from the heating process. The first and second crystallization onset and peak temperatures are labeled as T_{x1}, T_{x2}, T_{p1} and T_{p2}, respectively. The first exothermic peak (T_{p1}) corresponds to the crystallization of α-Fe phase [8,18] and the second one (T_{p2}) corresponds to that of Fe–P compounds [11]. It should also be noted that the onset temperature T_{x1} of the first crystallization process decreases slightly from 632 K to 626 K while there is an obvious increase of T_{x2} from 652 K to 661 K with the increase of Al content. The temperature interval $\Delta T_x = (T_{x2} - T_{x1})$ are shown in Fig. 2(b) as a function of Al content. One can see that the ΔT_x increases as Al content increases, which agrees well with that observed in $Fe_{73.5-x}Al_xSi_{17.5}B_5Cu_1Nb_3$ ($x = 0$–1) [19]. The large temperature interval ΔT_x is beneficial to obtain an uniform nanocrystalline structure without the appearance of Fe-metalloid compounds with high magnetocrystalline anisotropy which is detrimental to achieve good soft magnetic properties [20,21]. The interval between the two onset temperatures of the two related crystallization processes enlarges with the increase of Al content from 20 K for S1 to 35 K for S4, which indicates that Al addition is able to enhance the thermal stability of nanocrystalline alloy to a certain extent [19,22], as the large ΔT_x benefits the formation of α-Fe nanocrystalline and inhibits the precipitation of non-ferromagnetic phases which deteriorate the soft-magnetic properties of the materials.

Fig. 3(a) shows the DSC curves of S3 amorphous ribbon examined at various heating rates (5, 10, 15, 20 K/min) in Ar atmosphere. Two exothermic peaks shift to high temperatures with the increase of heating rate. Activation energies of both the exothermic peaks can be gotten by using Kissinger equation [23],

$$\ln\left(\frac{\beta}{T_p^2}\right) = -\frac{E}{RT_p} + Const$$

where β is the heating rate, R is the universal gas constant, T_P is the specific absolute temperature of a given peak. Thus E can be gained from the slope of a straight line indirectly. Two Kissinger plots are shown in Fig. 3(b). The obtained activation energies E_{p1} and E_{p2} are 219 kJ/mol and 276 kJ/mol, respectively, while those of S1 ribbon are 238 kJ/mol and 224 kJ/mol, respectively [11]. Compared with S1, for S3 alloy activation energy of α-Fe phase has decreased 8.0% and that of Fe–P phase has increased 23%. Lower activation energy E_{p1} for alloys with higher Al content means worse GFA since in these alloys the crystallization process only needs to overcome a lower energy barrier [24], which is consistent with the XRD analysis. The increasement of energy E_{p2} indicates that the addition of Al greatly increases the activation energy of Fe–P phase crystallization in S3 amorphous ribbon, which means that in this alloy Fe–P phase is more difficult to emerge than in the Al-free alloy. Moreover, for S3 amorphous alloy the larger crystallization activation energy of Fe–P hard magnetic phase and smaller energy of the α-Fe soft magnetic phase guarantees that one can get the ribbon with partly nanocrystalline α-Fe phase from single-roller melt spinning method directly without Fe–P phase. In order to confirm that the compound appeared above T_{p2} is Fe_3P phases, we annealed the $Fe_{83}P_{15}Cu_1Al_1$ ribbon at 623 K for 150 s and XRD patterns of it on both free and wheel sides are shown in Fig. 4. From Fig. 4 one can see three peaks corresponding to (112), (411) and (222) of Fe_3P phase.

Fig. 5(a) and (b) show typical nanoindentation load–displacement (P–h) curves of melt-spun ribbons of free side and wheel side

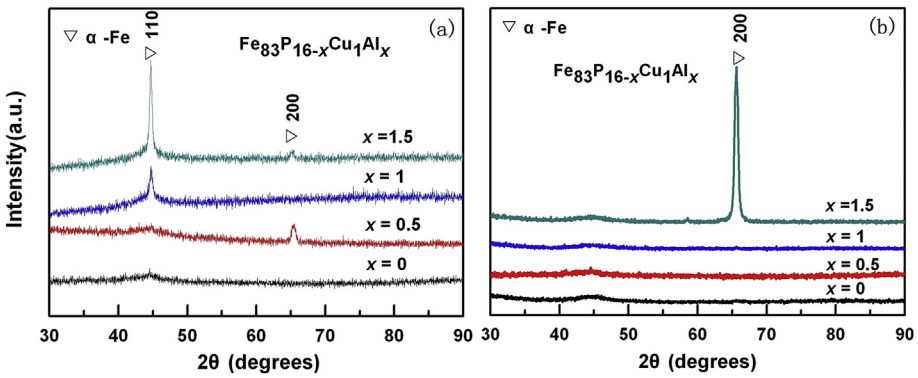

Fig. 1. XRD patterns of melt-spun $Fe_{83}P_{16-x}Cu_1Al_x$ (x = 0–1.5) alloy ribbons of the free side (a) and the wheel side (b).

Download English Version:

https://daneshyari.com/en/article/1606440

Download Persian Version:

https://daneshyari.com/article/1606440

Daneshyari.com